Nuclear Inst. and Methods in Physics Research, A 908 (2018) 198–205

Contents lists available at ScienceDirect

Nuclear Inst. and Methods in Physics Research, A

journal homepage: www.elsevier.com/locate/nima

Operation of the prospective beamline calorimeter in the high-radiation forward environment of the international linear collider☆

Bruce A. Schumm *, Benjamin Smithers

Santa Cruz Institute for Particle Physics and the University Of California, Santa Cruz, Santa Cruz, CA, 95064, United States

ARTICLE INFO

Keywords:
Radiation damage
Silicon diode sensor
Forward calorimetry

ABSTRACT

Results on electromagnetically-induced radiation damage to silicon diode sensors, obtained from the T506 experiment at SLAC, are used in concert with detailed shower simulations to project the effects of radiation damage on the proposed International Linear Collider Beamline Calorimeter (BeamCal) detector system. The study makes use of the FLUKA Monte Carlo to simulate electromagnetic showers in both the T506 apparatus and the prospective BeamCal detector system. Under the conservative assumption that damage leading to sensor leakage currents is dominated by the neutron component of the electromagnetic shower, and assuming that resulting leakage currents depend linearly on neutron fluence, the power consumption required to operate the BeamCal detector at a temperature of −10° C would be expected to increase by approximately 100 W per year of operation. Lowering the operating temperature to −30 °C would be expected to reduce the growth in power consumption to approximately 10 W per year. Under other assumptions about the source of damage, the accumulated power draw would be expected to be significantly less. Results on fluences of both electromagnetic and hadronic particles in regions peripheral to the bulk of the BeamCal detector system, where front-end electronics would be mounted, are also presented.

1. Introduction

The International Linear Collider (ILC) [1] is designed to collide beams of high energy electrons and positrons for the purpose of performing precision measurements of the properties of Standard Model particles and interactions, as well as to search for signatures of new physics that are otherwise difficult to detect. Among such signatures are those for which the new physics is only accessible through states that are nearly degenerate to long-lived neutral states that carry off most of the collision energy. Such signatures are produced in competition with high cross section two-photon events for which the incoming electron and positron are only slightly deflected in the collision, leading to a minimal energy deposition in the central detector that mimics the limited visible energy of the degenerate new physics signatures.

Such background events can, in principle, be identified and rejected if one or more of the deflected beam particles are identified in the most forward system of the ILC detector: the prospective Beamline Calorimeter (BeamCal), which provides coverage at angles as close as five milliradians from the beam trajectory. However, for nominal ILC collision parameters [1], this instrument would absorb approximately 10 TeV of electromagnetic particles per beam crossing, arising from the tens of thousands of electron–positron pairs created with each beam crossing. At the most irradiated point within the BeamCal, the accumulated radiation dose is expected to exceed 100 Mrad of ionizing radiation per year.

Envisioned as a sampling calorimeter with a tungsten absorber, the chosen sensor material must withstand the intense ionizing particle fields induced by the pair background showering in the tungsten. Potentially more damaging, though, is the flux of neutrons that arise primarily from the de-excitation of the 14 MeV giant dipole resonance of the tungsten nuclei [2] that is stimulated by the absorption of photons in the shower that are close to tungsten's 8 MeV critical energy. The associated radiation dose can lead both to the development of leakage current, resulting in quiescent power draw, as well as a loss of signal-collection efficiency.

To assess the damaging effect of tungsten-induced electromagnetic showers on various candidate solid-state sensor materials, the Santa Cruz Institute for Particle Physics (SCIPP) conducted experiment T506 in the SLAC End Station A Test Beam (ESTB) facility. In this experiment, for which results have been reported elsewhere [3], a multi-GeV electron beam was directed onto a tungsten radiator, in the midst of which (at shower max) a series of candidate sensors were inserted and exposed to doses of up to 600 Mrad of electromagnetically induced ionizing radiation. While the use of a tungsten radiator to surround the candidate sensor produced a realistic shower, containing both electromagnetic and hadronic components, both the energy and angular profile of the T506 radiation field, as well as the overall exposure rate, are different from that of the radiation field expected to illuminate the BeamCal. The purpose of this study was to use the FLUKA simulation package [4–6], combined with conventional assumptions about the radiation field

☆ Work performed within the FCAL Collaboration.

* Corresponding author.
E-mail address: baschumm@ucsc.edu (B.A. Schumm).

https://doi.org/10.1016/j.nima.2018.08.024
Received 10 May 2018; Received in revised form 7 August 2018; Accepted 8 August 2018
Available online xxxx

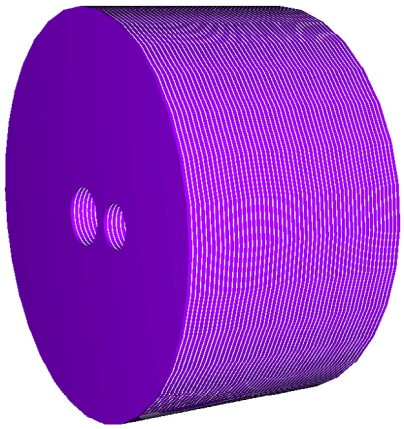

Fig. 1. Geometry of the BeamCal within the FLUKA simulation. This plot was produced using the visualization package within SimpleGeo [9].

energy profile dependence and the exposure dependence of the observed T506 damage, to estimate the effects of the pair-background-induced radiation field on the performance of a BeamCal constructed with silicon diode sensors. The simulation results will be presented in general enough form that radiation damage studies of other materials, whether from T506 or other experiments, can also be used to estimate the performance of those materials under prolonged use in the BeamCal.

2. The ILC and the beamline calorimeter

The International Linear Collider (ILC), if constructed, is expected to collide trains of beams of high-energy electrons and positrons at a rate of 5 Hz. The design energy, bunch separation within the train, number of bunches within a train, and bunch charge are subject to change as the design of the ILC matures and evolves to meet sharpening physics goals as well as practical and political constraints. For this study, we assume the baseline parameters presented in the Technical Design Report [1], for which a train consists of 1312 colliding bunches, each separated by 554 ns from the preceding bunch collision, and with a luminosity of 2.7 μb^{-1} per bunch collision. The flux of electron and positron pairs arising from the bunch collisions is simulated with the GUINEA-PIG [7] Monte Carlo program, initialized to reflect the collision parameters of the TDR baseline beam.

The current baseline design for the ILC Beamline Calorimeter (BeamCal) consists of a tungsten sampling calorimeter read out by planes of solid-state pad detectors. The calorimeter is composed of 50 tungsten plates of thickness 2.5 mm, with a radius (in the plane transverse to the beam direction) of 15 cm [8]. In the version simulated here, each plate is punctuated by two circular holes, one each to accommodate the incoming and outgoing beampipes, which diverge from each other with an angle of 14 mrad in the plane formed by the horizontal (x) and beam (z) axes. The hole accommodating the incoming beampipe has a radius of 1.55 cm, while the hole accommodating the outgoing beampipe has a radius of 2.05 cm, somewhat larger than that of the incoming beampipe to allow for the effects of disruption when the beams collide. At the face of the BeamCal (surface facing the ILC interaction point), the centers of the two holes are separated by 4.57 cm. The BeamCal is centered on the outgoing beamline at a distance of 326.5 cm from the interaction point, providing an angular coverage between 5 and 45 mrad. Fig. 1 depicts the basic geometrical features of the BeamCal.

3. The T506 experiment

The T506 Experiment, whose results on the radiation damage to solid-state sensors provide the empirical input to the FLUKA-based estimates of BeamCal degradation during operation at the ILC, was mounted in the SLAC National Accelerator Laboratory's End Station A Test Beam (ESTB) facility. The T506 target consisted of a 2 radiation length (X_0) upstream tungsten radiator (R1) that initiated the shower, followed after an air gap of 46 cm by a 4 X_0 tungsten radiator (R2) that brought the electromagnetic shower to maximum intensity. The candidate sensor was mounted immediately behind R2, followed immediately in turn by an 8 X_0 tungsten radiator (R3). The locations and thicknesses of the 10×10 cm^2 T506 target elements, which were produced with a tungsten purity of greater than 96%, are provided in Table 1. Mounting the sensor in the immediate proximity of tungsten radiators ensured that a significant hadronic component accompanied the electromagnetic particles in the shower.

Table 1
Location of the various tungsten radiator elements and the sensor under irradiation for the phase of T506 running in which the WSI-P4 sensor was irradiated. The R1 radiator had a thickness of 2 X_0, the R2 radiator 4 X_0, and the R3 radiator 8 X_0.

Surface	Location (cm)
R1 Entrance	0.0
R1 Exit	0.7
R2 Entrance	46.6
R2 Exit	48.0
Sensor	48.5
R3 Entrance	49.4

Target dose rates, as a function of electron beam energy and current, were estimated by using the Electron-Gamma-Shower (EGS) Monte Carlo program [10] to simulate the flux of particles in showers induced by the radiator configuration that pass through the candidate sensor location. To check the dose-calibration simulation, an in-situ measurement of the dose rate provided by a 0.75 nA beam of 4.02 GeV electrons was made using a REM Oxford Limited REM TOT601B radiation-sensing field-effect transistor positioned at the same location as that of the candidate sensors. This measurement provided a ~10% confirmation of the dose rates derived from simulation.

Sensors were characterized both before and after irradiation using a charge-collection (CC) apparatus at SCIPP on the UC Santa Cruz campus. The SCIPP CC apparatus incorporates a ^{90}Sr source that has a secondary β-decay with an end-point energy of 2.28 MeV that illuminates the sensor under study, passing through to a scintillator immediately behind the sensor that is read out by a photomultiplier tube. For assessing the CCE of pad sensors, a two-stage, single-channel amplifier was constructed from discrete components, based on a design of Fabris, Madden and Yaver [11], and shaped to a rise time of 290 ns. Upon receiving a trigger from the scintillator, the signal from the amplifier was read out by a Tektronix DPO 4054 digital storage oscilloscope, and the digitized waveforms were written out and stored on the disk of a dedicated data-acquisition computer. Since not all β particles that trigger the scintillator go through the pad, the resulting pulse-height distribution shows contributions from both the Landau deposition of the through-going β particles, as well as that of the noise pedestal, allowing for an in-situ subtraction of the mean pedestal. The width of the pedestal distribution then provides a measurement of the readout noise, which was found to be approximately 250 electrons at room temperature for un-irradiated sensors. Bias voltage and leakage current measurements were provided by a Keithley 237 High Voltage Source Measurement Unit. The environmental state within the freezer was monitored with a Sper Scientific 8000014 Humidity/Temperature Datalogger. More details about the exposure of candidate sensors, and their characterization both before and after irradiation, can be found in [3].

Of particular interest to this work was the 2015 exposure of sensor WSI-P4, a $1.6 \times 1.6 \times 0.32$ mm^3 p-type float-zone bulk pad-diode test structure associated with a prototype sensor developed for the ATLAS upgrade tracker [12]. In this exposure, 51 μC of 13.3 GeV electrons were directed onto the T506 target over a period of approximately one day, corresponding to an accumulated dose of ionizing radiation

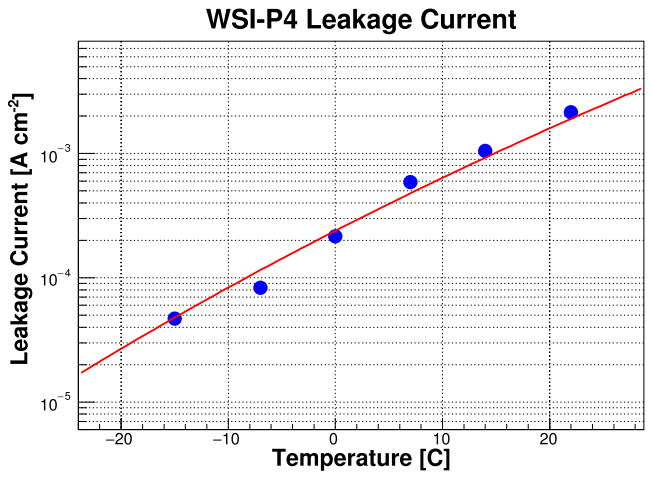

Fig. 2. Observed temperature dependence of the area current density of the WSI-P4 silicon diode sensor biased at 600 V, after irradiation. The fit is to the function of the form of Eq. (1).

of approximately 270 Mrad. The sensor was irradiated at close to 0 °C and kept well below freezing subsequent to irradiation. A reverse bias of 10 V was applied to the sensor during irradiation to draw off any accumulated static charge. The sensor's leakage current and charge collection efficiency were then evaluated after a series of one-hour annealing steps at room temperature, 40 °C, 50 °C, and finally 60 °C. While the post-irradiation leakage current was not changed significantly by the annealing episodes after the first (room temperature) annealing step, subsequent annealing steps were observed to lower the bias voltage required to reach a plateau in the charge collection efficiency. At a bias of 600 V, close to the bias voltage required for maximum charge collection after the 60 °C annealing step, the charge collection efficiency was observed to be 80% of its un-irradiated value. The area density $\sigma(T)$ of the leakage current for the irradiated WSI-P4 sensor, at a bias of 600 V, is displayed as a function of temperature in Fig. 2. Under the assumption that the leakage current is due to displacement damage in the silicon bulk, the temperature dependence is expected to follow the quasi-empirical relation [13]

$$I(T) \propto T^2 e^{-E_{\text{eff}}/2kT}, \tag{1}$$

where T is the sensor operating temperature in degrees kelvin, and $E_{\text{eff}} = 1.21$ eV is an effective trap energy gap parameter. The fit to the data shown in the figure follows this form, and with a constant of proportionality of 4.7×10^2 A/cm$^2 K^2$ provides a good description of the data over the measured range of temperature. This dependence will be made use of in the estimates of the power draw of the irradiated BeamCal presented below.

4. FLUKA simulation and the exposure metric

Both the T506 target and BeamCal design were implemented in FLUKA. To enable neutron production through the evaporation of excited nuclear resonances, the "SDUM" argument for the FLUKA "PHYSICS" control card was set to the value "EVAPORAT"; the new FLUKA model of evaporation without heavy fragmentation was implemented through the use of the value "2" for the "WHAT(1)" argument of the "PHYSICS" card. To provide the maximum precision in the modeling of neutrons arising within the electromagnetic shower, the "SDUM" argument was set to the value "PRECISIO" for the "DEFAULTS" card. Photonuclear interactions themselves were enabled by activating all available options of the "PHOTONUC" card. With FLUKA configured in this manner, low-energy neutron transport was modeled down to thermal energies. These settings are summarized in Table 2.

Table 2
Values of relevant FLUKA configuration parameters used in this study.

FLUKA Card	Option	Value
PHYSICS	SDUM	EVAPORAT
PHYSICS	WHAT(1)	2
DEFAULTS	SDUM	PRECISIO
LAM-BIAS	WHAT(2)	+0.09
PHOTONUC	[All Options]	Enabled

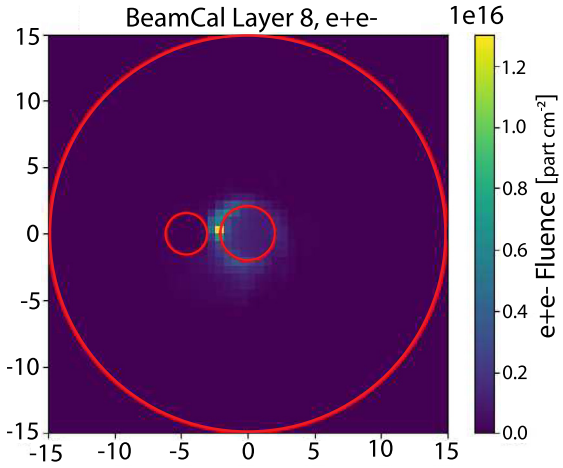

Fig. 3. Estimated electromagnetic (electron and positron) fluence, in cm^{-2}, at the maximum of the electromagnetic shower in the BeamCal, per 10^7 s of ILC operation. The estimated maximum occurs in the eighth sensor layer. The outer red circle represents the periphery of the BeamCal, while the larger (smaller) red circles represent the exit (entrance) holes for the ILC beams, also visible in Fig. 1. Distances are in cm.

The model of the T506 target that was implemented in the FLUKA simulation is described in Table 1. FLUKA was then used to simulate 3×10^5 electromagnetic showers induced by incident electrons of energy 13.3 GeV. To simulate the rastering of the target during the T506 exposure, the incident flux was distributed evenly within a square of side one cm, oriented transverse to the incident beam direction.

The BeamCal device was modeled as a set of 50 alternating layers of pure tungsten plates of thickness 2.5 mm and pure silicon sensors of thickness 300 μm, with each tungsten plate separated by 700 μm. Showers from electrons and positrons expected to arise from a single ILC beam crossing, assuming the nominal beam parameters [1], were simulated. The incident electron/positron flux consisted of approximately 5×10^4 incident charged particles, with a mean energy of 2.5 GeV and a high-energy tail extending to beyond 100 GeV. The simulated flux of particles incident on the BeamCal was highly peaked in the plane transverse to the beam direction, with the maximum of the distribution falling close to the inner edge of the exhaust beam cutout. The simulated electromagnetic flux in the 8th sensor layer, close to the peak of the resulting distribution of electromagnetic shower particles, is shown in Fig. 3.

The FLUKA simulation provides an accounting of the fluence Φ of particles traversing a given "scoring plane" of finite area A and infinitesimal width dz, with the fluence Φ defined as

$$\Phi = \lim_{dz \to 0} \frac{l}{A dz}, \tag{2}$$

where l is the sum of all path lengths traversing the scoring plane's infinitesimal volume $A dz$. A single particle with angle of incidence θ passing through a scoring plane of area A thus represents a fluence of $\Phi = 1/(A \cos\theta)$, with a physical unit of cm^{-2}. FLUKA can be configured to provide the differential fluence distribution in a two-dimensional grid of energy (E) and angle of incidence (θ) of shower particles relative to the normal of the scoring plane.

According to the non-ionizing-energy-loss (NIEL) scaling hypothesis [14], radiation damage in solid-state sensors is proportional to

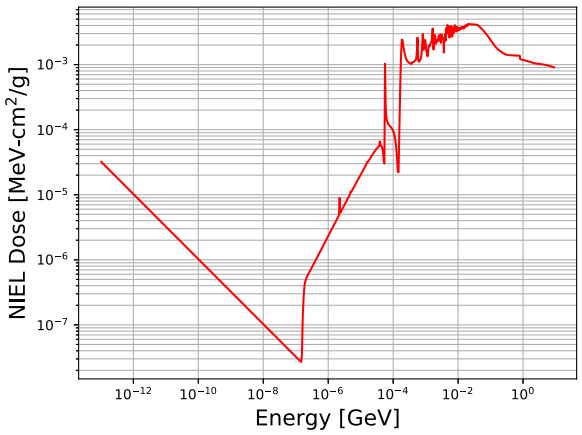

Fig. 4. Energy dependence of neutron-induced NIEL in silicon, in MeV per g/cm^2 of silicon traversed per through-going neutron.
Source: This plot displays the data tabulated in [14].

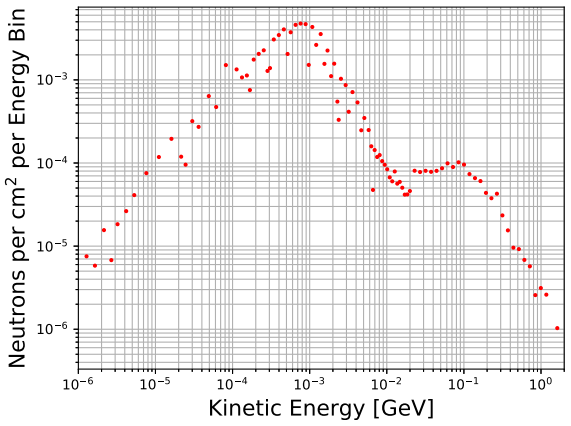

Fig. 5. FLUKA estimate of the neutron fluence per 13.3 GeV primary electron, as a function of incident neutron energy, through the sensor scoring plane for the T506 experiment. The total estimated per-primary neutron fluence is given by the sum of the bin contents.

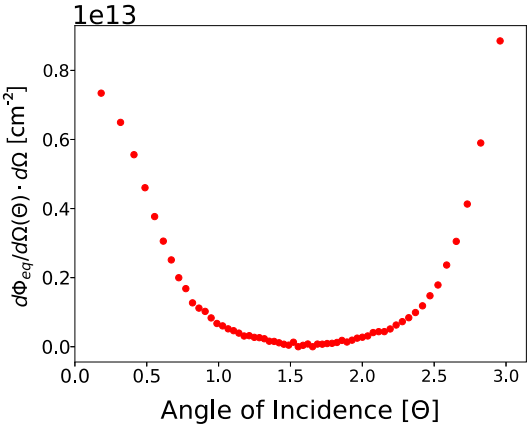

Fig. 6. FLUKA estimate of the angular dependence of the 1 MeV-equivalent neutron fluence through the sensor scoring plane for the full exposure of the T506 experiment.

the deposition of energy in the sensor through processes other than ionization, i.e., processes in which the nuclei, rather than the electronic states, absorb energy from the incident radiation. In this study, we are interested in the effects of NIEL arising from the flux of neutrons that originate within the electromagnetic shower itself. Because the production of these neutrons is largely due to the excitation of the giant dipole resonance, whose predominantly evaporative decay produces an isotropic distribution of neutrons relative to the decaying nucleus, the neutron-induced NIEL dose is much more pervasive within the BeamCal device than is the more ballistic electromagnetically-induced NIEL dose. An assumption that the radiation damage observed in T506 is dominated by neutron-induced NIEL is thus conservative with respect to the projected performance of the BeamCal after exposure to radiation.

The neutron-induced NIEL dose $N_n(E)$ per unit path length depends on the energy of the through-going neutron. The function $N_n(E)$ is well known for neutrons passing through silicon, and is tabulated in [14] in terms of MeV of neutron-induced NIEL per g/cm^2 of silicon traversed per through-going neutron (see Fig. 4). The quantity $\rho N_n(E)$, where $\rho = 2.33$ g/cm^3 is the mass density of silicon, thus provides the neutron-induced NIEL in terms of MeV per cm of traversed silicon. For a given bin of extent $\Delta E \Delta\Omega$ centered around an energy E and incident angle θ of neutrons traversing the scoring volume, the contribution ΔE_{NIEL} to the neutron-induced NIEL in the scoring plane volume is thus given by

$$\Delta E_{\text{NIEL}} = \rho N_n(E) \frac{d^2 l}{dE d\Omega}(E,\theta) \Delta E \Delta\Omega \tag{3}$$

in units of MeV of neutron-induced NIEL; again, l is the total path length of neutrons through the scoring plane volume. More applicable, however, is the neutron-induced NIEL per unit of scoring plane volume due to neutrons in the given energy and angle bin, given by

$$\Delta\lambda = \lim_{dz\to 0} \frac{\Delta E_{\text{NIEL}}}{A dz} = \rho N_n(E) \frac{d^2\Phi}{dE d\Omega}(E,\theta) \Delta E \Delta\Omega \tag{4}$$

in units of MeV of neutron-induced NIEL per cm^3 of scoring-plane volume, which makes explicit use of the double-differential fluence distribution $d^2\Phi/dEd\Omega$ provided by FLUKA. Note that in this discussion of NIEL, the energy E is that of the given shower particle (neutron) that is incident on the scoring plane buried within the apparatus, and not the energy of the particle (electron or positron) that initiates the shower.

The total exposure λ, again in terms of MeV of neutron-induced NIEL per cm^3 of scoring-plane volume, is then given by summing over all bins in angle and energy:

$$\lambda = \sum_{i=1}^{N_{bins}} \rho N_n(E_i) \frac{d^2\Phi}{dE d\Omega}(E_i,\theta_i) \Delta E_i \Delta\Omega_i. \tag{5}$$

For this study, simulated neutrons incident upon the scoring plane were binned in 60 uniform bins of $\Delta\Omega$, each of width $\pi/15$, and 336 logarithmically-varying bins of energy between 1×10^{-5} eV and 100 GeV.

5. Estimated T506 neutron dose

The FLUKA simulation of the T506 geometry, as described above, was used to estimate the neutron-induced NIEL dose accumulated by the WSI-P4 sensor during its exposure in the T506 experiment. A total of 3×10^5 13.3 GeV electron showers were simulated with FLUKA. Fig. 5 shows the energy distribution of the simulated neutron flux, per incident 13.3 GeV electron, that traversed the sensor. Fig. 6 shows the differential neutron-induced NIEL dose distribution $d\Phi/d\Omega$ as a function of neutron angle of incidence for the FLUKA simulation of the full WSI-P4 exposure. Due to the ballistic nature of the electromagnetic shower, the neutron fluence arises primarily from the region of the 1 cm^2 beam profile in the radiator immediately before and after the WSI-P4 sensor. As a result, the dose distribution is dominated by neutrons entering either the front or the back of the sensor with lower angles of incidence. Summing over all incident angles, and scaling to the delivered charge of 51 μC of 13.3 GeV electrons, yields an estimate of the total neutron-induced NIEL dose of

$$\lambda_{T506} = 2.7 \times 10^{11} \ \text{MeV/cm}^3 \tag{6}$$

in the WSI-P4 sensor, referred to below in comparisons with the projected BeamCal dose as the "T506 dose unit".

6. Expected WSI-P4 current draw (neutron dominance)

As a point of comparison, studies of silicon diode detector leakage current arising from hadronic irradiation have been performed by the CERN RD48 Collaboration [15]. RD48 explored a broad range of silicon diode detector technologies exposed to varying levels of irradiation, and found a consistent linear dependence of the leakage current draw upon radiation dose. In terms of the 1-MeV equivalent neutron fluence Φ_{eq}, defined as

$$\Phi_{eq} = \int \frac{d\Phi}{dE}(E)\frac{N_n(E)}{N_n(1\text{MeV})}dE, \tag{7}$$

RD48 found that operating at a temperature of 20 °C after an 80 min annealing step at 60 °C, the current draw in amps for a fully-depleted sensor could be approximated as

$$I = \alpha\Phi_{eq}V, \tag{8}$$

where V is the volume of the sensor bulk in cm^3, and with the current proportionality constant α given by

$$\alpha^{+20}_{RD48} = 4.0\times10^{-17}\ \text{A/cm}. \tag{9}$$

Making use of the expected displacement-damage leakage-current temperature dependence (Eq. (1) from Section 3), the current proportionality constant for an operating temperature of −10 °C would be

$$\alpha^{-10}_{RD48} = 2.1\times10^{-18}\ \text{A/cm}. \tag{10}$$

The FLUKA simulation of the T506 target, combined with the energy-dependent neutron-induced NIEL values from [14], yielded an estimate of $\Phi_{eq} = 0.19\ \text{n}_{eq}/\text{cm}^2$ per 13.3 GeV primary, leading to an estimate of

$$\Phi^{\text{T506}}_{eq} = 6.0\times10^{13}\ \ \text{n}_{eq}/\text{cm}^2 \tag{11}$$

for the 51 μC WSI-P4 exposure. Based on the assumption of neutron-dominated radiation damage, and the results of the RD48 leakage-current studies, this leads to an expectation of 4.0 μA/cm^2 for the 320 μm-thick WSI-P4 sensor, operating at a temperature of −10 °C. From Fig. 2, the current observed in the WSI-P4 sensor at −10 °C was 83 μA/cm^2; at full depletion, this value would be slightly higher.

Thus, based on the results of RD48 studies, the observed current draw for the WSI-P4 sensor is significantly greater than that expected from the assumption of neutron-dominated radiation damage. It is thus quite possible that the radiation damage observed in the WSI-P4 sensor is caused predominantly by components of the electromagnetic shower other than the neutron flux.

It should also be noted that the WSI-P4 ionizing-radiation dose of 270 Mrad corresponds to a charged-particle fluence Λ_{T506} of

$$\Lambda_{T506} = 1.1\times10^{16}\ \ e^{\pm}/\text{cm}^{-2}. \tag{12}$$

Assuming an electron-induced NIEL factor of 1.3×10^{-4} MeV-cm^2/g [16], this corresponds to a charged-particle-induced NIEL dose of approximately 3.3×10^{12} MeV/cm^3, an order of magnitude larger than that expected from neutrons (see Eq. (6)). Thus, it is possible that the charged-particle (electron/positron) component of the tungsten-induced showers provides the dominant source of radiation damage to the WSI-P4 sensor. Since, relative to the photon and neutron component, this charged-particle component is the most ballistic, and thus falls off most quickly with distance from the center of the BeamCal, the assumption that the T506 leakage current results are dominated by damage from charged particles will lead to the smallest estimated power-draw accumulation during operation. Power-draw estimates for the assumption of charged-particle dominance are presented below in addition to those for the assumption of neutron dominance.

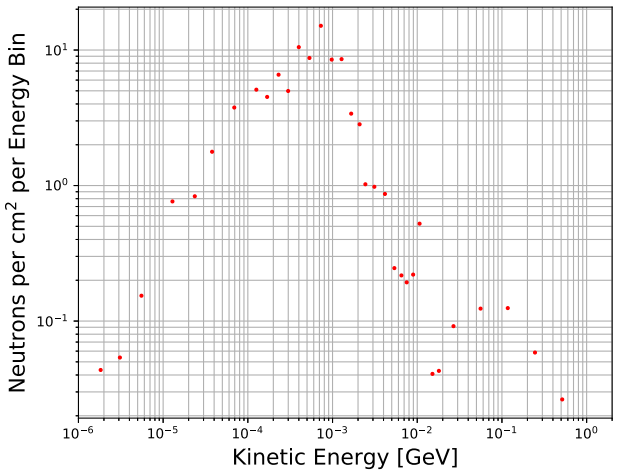

Fig. 7. FLUKA estimate neutron flux, as a function of incident neutron energy, through the sensor scoring plane for Layer 12 of the BeamCal, per ILC beam crossing. The distribution shown is that for a scoring plane centered on the maximum of the electromagnetic component (see Fig. 3). The total estimated per-crossing neutron fluence is given by the sum of the bin contents.

7. BeamCal neutron-induced NIEL distribution

The FLUKA package was used, as described above, to simulate the neutron field over the breadth and depth of the prospective ILC Beamline Calorimeter. The resulting energy distribution of neutrons for Layer 12 of the BeamCal, for a scoring plane centered on the maximum of the electromagnetic component of the expected shower profile (see Fig. 3), is shown in Fig. 7. Layer 12 is close to the peak depth of the neutron fluence distribution for the ILC-induced showers. The neutron energy distribution is very similar to that observed for the T506 scoring plane (Fig. 5).

Figs. 8 and 9 (left) show the differential neutron-induced NIEL dose distribution $d\Phi/d\Omega$ as a function of neutron angle of incidence, per 10^7 s of ILC operation, for three locations in Layer 12 of the BeamCal. The three locations are widely separated, including a point in the center of the layer, as well as one 24.1 mm beyond the outer edge of the exhaust (larger) circular cutout and one 34.2 mm beyond the outer edge of the incoming (smaller) circular cutout. Fig. 9 (right) shows $d\Phi/d\Omega$ averaged over the entire layer. Reflective of the more distributed flux of electromagnetic particles on the face of the BeamCal, and the isotropic nature of the dominant source of neutrons in the shower (evaporative de-excitation of the giant dipole resonance in tungsten), the BeamCal neutron fluence distribution is much more evenly spread out over solid angle than that of the T506 fluence distribution (Fig. 6). As a result, the neutron fluence decreases much less rapidly with transverse distance from the axis of the shower peak than does the electromagnetic fluence. Should BeamCal radiation damage be dominated by this neutron flux, this may lead to a prohibitive dissipative heat load in the BeamCal after operation in the ILC beam. Results on the projected BeamCal power draw are presented in the next section.

A series of scoring planes was configured across a section of the BeamCal at the depths of Layers 12 and 30, including those represented in Figs. 8 and 9. For each scoring plane, the neutron-induced NIEL per ILC beam crossing was estimated. This result was then scaled up by the product of factors of 6560 (the number of ILC beam crossings per second) and 10^7 (the estimated number of second of operation per year) to provide an estimated neutron-induced NIEL per year of ILC operation. Figs. 10 and 11 show the neutron-induced NIEL results for these various scoring planes in Layers 12 and 30, respectively. The results are expressed in terms of the T506 dose unit λ_{T506} described above. The neutron-induced NIEL profile is seen to fall off much less rapidly with distance from the center of the BeamCal than the corresponding electromagnetically-induced deposition (see Fig. 3). Thus,

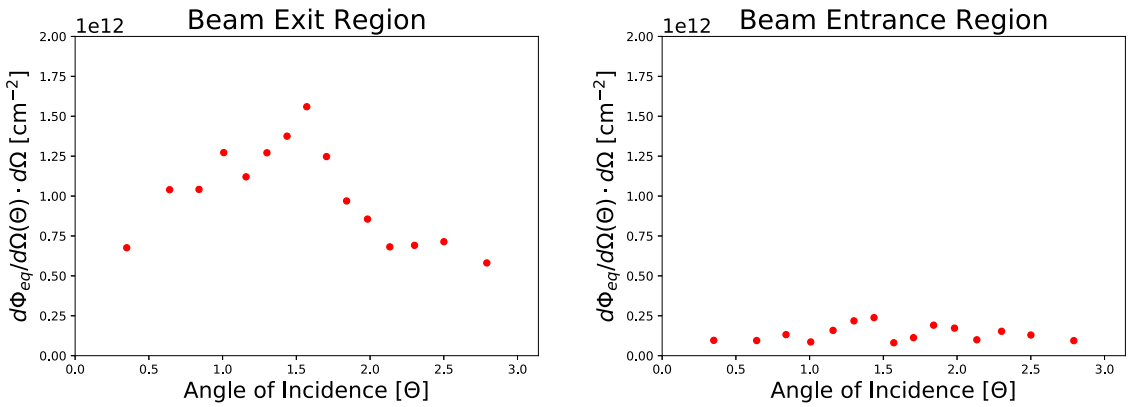

Fig. 8. FLUKA estimates of the angular dependence of the 1 MeV-equivalent neutron fluence through scoring planes in Layer 12 of the BeamCal, for 10^7 s of ILC operation. Left: fluence distribution for a scoring plane 24.1 mm beyond the outer edge of the exhaust (larger) circular cutout. Right: fluence distribution for a scoring plane 34.2 mm beyond the outer edge of the incoming (smaller) circular cutout.

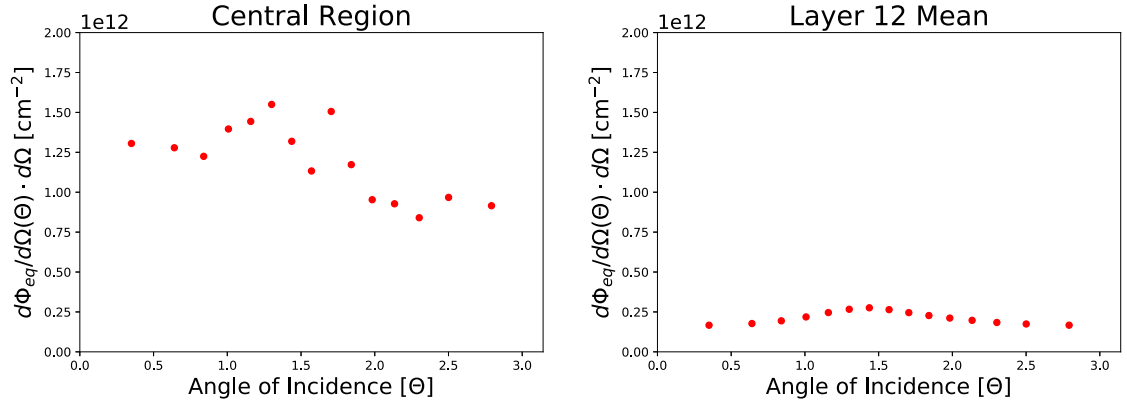

Fig. 9. FLUKA estimate of the angular dependence of the 1 MeV-equivalent neutron fluence through scoring planes in Layer 12 of the BeamCal, for 10^7 s of ILC operation. The distribution shown in the left plot is that for a scoring plane at the center of the BeamCal, i.e., at the peak of the electromagnetic flux shown in Fig. 3. The right plot shows the average of the distribution over the full layer.

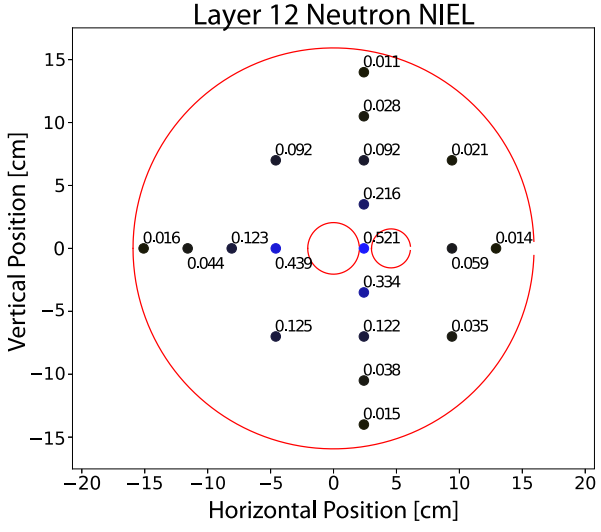

Fig. 10. FLUKA estimate of neutron-induced NIEL for the various scoring planes configured for Layer 12 of the BeamCal. The results are shown per year of ILC running (as defined in the text), and expressed in terms of the T506 dose unit λ_{T506}.

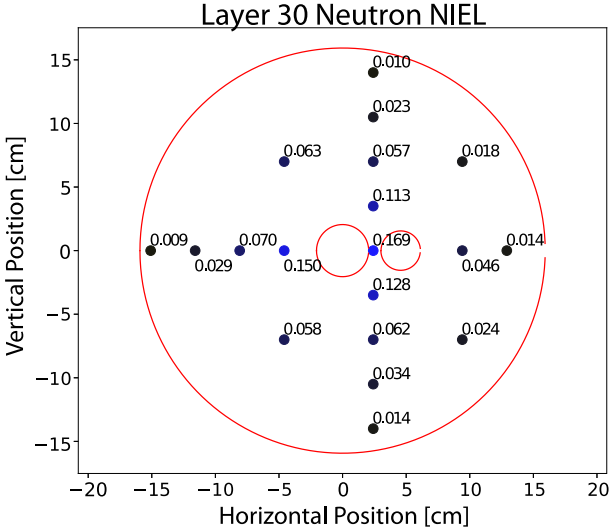

Fig. 11. FLUKA estimate of neutron-induced NIEL for the various scoring planes configured for Layer 30 of the BeamCal. The results are shown per year of ILC running (as defined in the text), and expressed in the T506 dose unit λ_{T506}.

as mentioned above, an assumption that the leakage-current inducing radiation damage observed in the T506 experiment is dominated by neutron-induced NIEL is conservative with respect to the total estimated leakage current (and resulting power draw) for the irradiated BeamCal.

8. Expected power draw after irradiation: neutron dominance

By introducing a single scoring plane incorporating the entire surface of a given BeamCal layer's sensor plane, FLUKA can be configured to

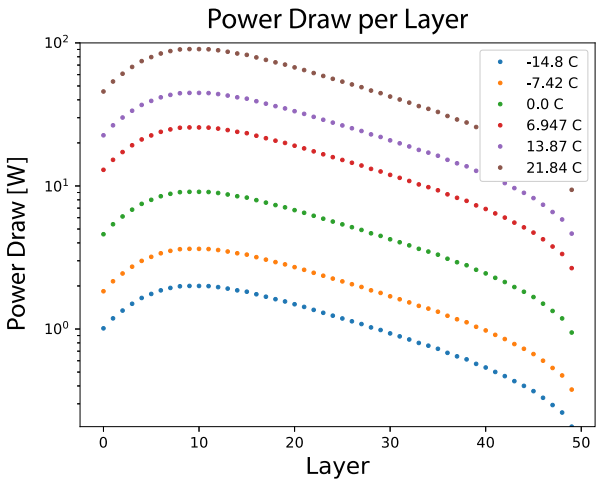

Fig. 12. Expected power draw per layer for operation with a bias voltage of V_B = 600 V after 10^7 s of operation in the ILC, for various operating temperatures, under the assumption of neutron dominance.

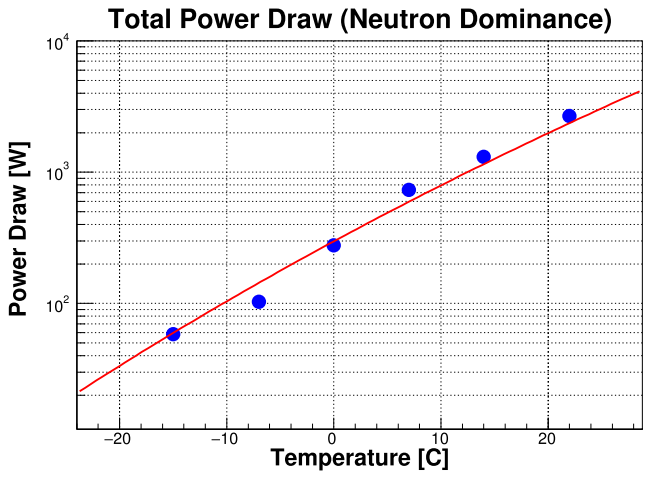

Fig. 13. Expected power draw as a function of temperature for the entire BeamCal after 10^7 s of operation at the ILC, for operation with a bias voltage of V_B = 600 V, under the assumption of neutron dominance.

accumulate the mean differential neutron fluence $d^2\Phi_L/dEd\Omega$ through the entire detector layer for a given duration of ILC operation with nominal beam parameters. This can then be converted to a mean neutron-induced NIEL energy-deposition density λ_L as outlined in Section 4. Assuming neutron-dominated radiation damage, and a linear dependence of leakage current upon neutron-induced NIEL dose, the total leakage current through the given layer, for a bias of V_B = 600 V and an operating temperature T, can then be estimated as

$$I_L(T) = \frac{\lambda_L}{\lambda_{T506}} A\sigma(T), \tag{13}$$

where A is the sensor surface area, $\sigma(T)$ is the area current density measured for the irradiated WSI-P4 sensor (see Fig. 2), and λ_{T506} = 2.7×10^{11} MeV/cm^3 is the neutron-induced NIEL dose accumulated by the WSI-P4 sensor. Here, it is assumed that the thickness of the BeamCal sensor is approximately the same as that of the WSI-P4 sensor (320 μm). The total power draw $P_L(T)$ in the layer is then given by multiplying the current draw $I_L(T)$ by the bias voltage:

$$P_L(T) = V_B I_L(T) = V_B \frac{\lambda_L}{\lambda_{T506}} A\sigma(T). \tag{14}$$

Fig. 12 show the resulting estimate for $P_L(T)$ as a function of layer for a series of operating temperatures between −15 °C and 22 °C, for 10^7 s of operation at the ILC. Replacing the T506 observed leakage current dependence $\sigma(T)$ with the RD48 expectation for neutron-damage leakage currents (see Section 6) would lower the power draw estimate by roughly a factor of 20 over the displayed range of temperature.

The maximum power dissipation density will arise approximately at the peak of the electromagnetic (electron and positron) deposition distribution in Layer 12 of the BeamCal. At this point, after 10^7 s of exposure in the ILC and operating at a bias voltage of 600 V and a temperature of −10 °C, under the assumption of neutron-dominated radiation damage the power draw is expected to be approximately 25 mW per cm^2 of sensor area.

Having estimated the layer-by-layer current draw as a function of operating temperature, the total power draw is then given by summing the power draw over all layers. Fig. 13 shows the total expected power draw as a function of temperature; under the assumption of neutron-dominated radiation damage, the expected power draw after roughly 1 year of ILC operation varies between 30 and 2000 W for temperatures between −20° and 20 °C, and would be of order 10 W for an operating temperature of −30 °C.

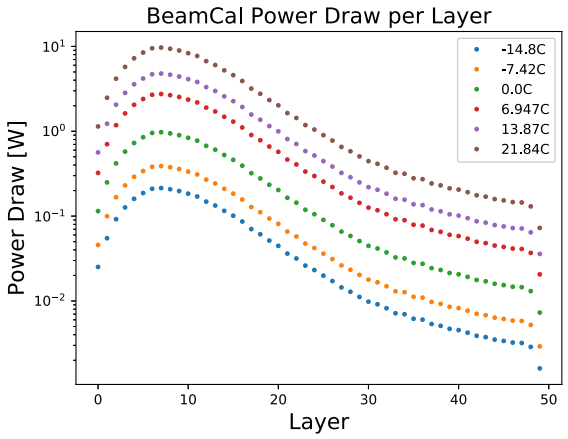

Fig. 14. Expected power draw per layer for operation with a bias voltage of V_B = 600 V after 10^7 s of operation in the ILC, for various operating temperatures, under the assumption of charged-particle dominance.

9. Expected power draw after irradiation: charged-particle dominance

The estimation of the power-draw accumulation for the assumption of charged-particle dominance parallels that of the case of neutron dominance. A single scoring plane per layer is used to accumulate the mean charged-particle fluence Λ_L per BeamCal layer, per 10^7 s of ILC operation. The expected power draw in the layer, under the assumption of charged-particle dominance, is then given by

$$P_L^{ch}(T) = V_B \frac{\Lambda_L}{\Lambda_{T506}} A\sigma(T), \tag{15}$$

where Λ_{T506} is the estimated total charged-particle fluence through the WSI-P4 sensor introduced in Section 6.

Fig. 14 shows the resulting estimate for $P_L^{ch}(T)$ as a function of layer for a series of operating temperatures between −15 °C and 22 °C, for 10^7 s of operation at the ILC. The maximum power dissipation density under the assumption of charged-particle dominance, for a bias voltage of 600 V and an operating temperature of −10 °C, is estimated to be approximately 10 mW per cm^2 of sensor area. Fig. 15 shows the total expected power draw as a function of temperature for the assumption of charged-particle dominance. Under this assumption, the expected power draw after roughly 1 year of ILC operation varies between 2 and 100 W

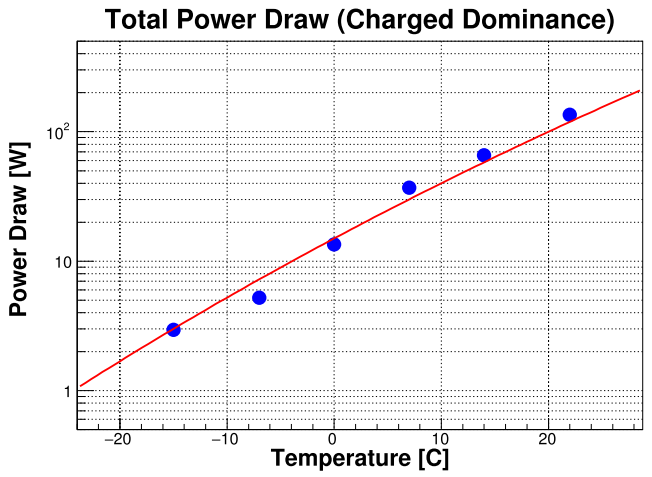

Fig. 15. Expected power draw as a function of temperature for the entire BeamCal after 10^7 s of operation at the ILC, for operation with a bias voltage of $V_B = 600$ V, under the assumption of charged-particle dominance.

Table 3
Neutron fluences at various positions 1 cm outside the BeamCal, for 10^7 s of ILC operation, in cm^{-2}. The angle is measured relative to the axis defined by the center of the BeamCal and the centerline of the smaller circular cutout. The small angular dependence arises from the asymmetries in the BeamCal geometry and electromagnetic energy deposition distribution visible in Fig. 3.

Angular position	0	$\pi/2$	π	$3\pi/2$
Layer 12 fluence (cm^{-2})	5×10^{11}	6×10^{11}	7×10^{11}	8×10^{11}
Layer 30 fluence (cm^{-2})	5×10^{11}	5×10^{11}	6×10^{11}	5×10^{11}

for temperatures between −20° and 20 °C, and would be well below 1 W for an operating temperature of −30 °C.

10. Peripheral flux calculations

The BeamCal front-end electronics is likely to be mounted just outside the BeamCal structure. Thus, FLUKA has also been used to estimate neutron and charged-particle fluences in regions immediately peripheral to the BeamCal.

Table 3 shows the expected neutron fluence per nominal year of operation, for scoring planes oriented transverse to the beam direction, at various points 1 cm outside the BeamCal. The corresponding electromagnetic fluence was found to be less than 10^{11} through-going charged particles (electrons and positrons) per cm^2 per nominal year at any of these positions, corresponding to an ionizing dose of less than 2.5 krad per year from this source.

11. Summary and conclusions

Making use of the FLUKA simulation package, projections have been made of the performance of the Beamline Calorimeter after exposure to beam-induced radiation from the prospective International Linear Collider. These projections were normalized to the observed performance of a prototype p-type, float-zone bulk prototype silicon diode pad detector exposed to tungsten-induced electromagnetic showers in experiment T506 at the SLAC End Station Test Beam facility.

The T506 studies suggest that after several years of exposure of a Beamline Calorimeter instrumented with silicon diode sensors, for sufficient bias voltage the charge collection will remain high (50% or greater) even in the most heavily-irradiated portions of the Beamline Calorimeter. Using the FLUKA simulation to estimate the T506 neutron dose, and neutron-induced leakage current results from the RD48 collaboration, the overall current draw is found to be higher than that expected for the assumption that observed T506 leakage currents are predominantly caused by radiation damage from the neutron component of the electromagnetic shower.

However, under the conservative assumption that the damage is neutron-induced, and assuming operation at a bias voltage of 600 V and a temperature of −10 °C, the overall power draw of the Beamline Calorimeter is expected to increase by approximately 100 W per year of operation. Lowering the operating temperature to −30 °C would be expected to reduce the growth in power consumption to approximately 10 W per year. Under the least-conservative assumption that the charged particle component dominates the radiation damage, the corresponding estimate is of order 5 W of power-draw accumulation per year of operation for an operating temperature of −10 °C. Further studies clarifying the source of radiation damage in tungsten-induced electromagnetic showers should allow this range to be substantially narrowed. Nonetheless, even under the conservative assumption of neutron-dominated radiation damage, a BeamCal design incorporating silicon diode sensors seems feasible.

Finally, both charged and neutral particle fluences in the region just outside the Beamline Calorimeter, where the front-end electronics would be mounted, were estimated to be at levels that would be unlikely to pose a threat to the performance of the readout.

Role of the Funding Source

The work described in this article was supported by the United States Department of Energy, grant DE-SC0010107. The funding agency played no role in the design, execution, interpretation, or documentation of the work described herein.

References

[1] T. Behnke, etal, [ILC Collaboration], The International Linear Collider Technical Design Report, 2013, arXiv:1306.6327 [physics.acc-ph].
[2] B.L. Berman, S.C. Fultz, Measurements of the giant dipole resonance with monoenergetic photons, Rev. Modern Phys. 47 (1975) 713.
[3] P. Anderson, et al., Updated results of a solid-state sensor irradiation study for ILC extreme forward calorimetry, in: Proceedings of the LCWS2016 International Workshop on Linear Colliders, Morioka City, Iwate, Japan, December 5–9, 2016, arXiv:1703.05429.
[4] A. Ferrari, P.R. Sala, A. Fassò, J. Ranft, FLUKA: A multi-particle transport code (program version 2005), CERN Yellow Report. https://cds.cern.ch/record/898301, 2005.
[5] T.T. Böhlen, et al., The FLUKA code: Developments and challenges for high energy and medical applications, CERN-2005-10, 2005, INFN/TC_05/11, SLAC-R-773.
[6] V. Vlachoudis, FLAIR: A powerful but user friendly graphical interface for FLUKA, in: Proc. Int. Conf. on Mathematics, Computational Methods & Reactor Physics, M&C 2009, Saratoga Springs, New York, 2009, http://www.fluka.org/flair/.
[7] D. Schulte, Study of Electromagnetic and Hadronic Background in the Interaction Region of the TESLA Collider, (Ph.D. thesis), DESY, 1997.
[8] P.N. Burrows, et al., SID detailed baseline design, http://www.desy.de/~stanitz/DBD-pac101212pdf, December 2013.
[9] C. Theis, et al., Interactive three dimensional visualization and creation of geometries for monte carlo calculations, Nucl. Instrum. Methods A562 (2006) 827, http://theis.web.cern.ch/theis/simplegeo/.
[10] The Electron Gamma Shower (EGS) Monte Carlo Program, http://rcwww.kek.jp/research/egs/.
[11] L. Fabris, N.W. Madden, H. Yaver, A fast, compact solution for low noise charge preamplifiers, Nucl. Instrum. Methods A 424 (1999) 545–551.
[12] Y. Unno et al, Development of n-on-p silicon sensors for very high radiation environments, Nucl. Instrum. Methods A 636 (2011) S24.
[13] A. Chilingarov, Temperature dependence of the current generated in si bulk, J. Instr. 8 (2013) P10003, http://dx.doi.org/10.1088/1748-0221/8/10/P10003.
[14] A. Vasilescu, G. Lindstroem, Displacement damage in silicon, on-line compilation, 2006, http://rd50web.cern.ch/RD50/NIEL/default.html.
[15] G. Lindström, et al., Radiation hard silicon detectors - developments by the RD48 (ROSE) collaboration, Nucl. Instrum. Methods A466 (2001) http://dx.doi.org/10.1016/S0168-9002(01)00560-5.
[16] M.J. Boschini, P.G. Rancoita, M. Tacconi, SR-NIEL calculator: Screened relativistic (SR) treatment for calculating the displacement damage and nuclear stopping powers for electrons, protons, light- and heavy- ions in materials (version 395), 2014, [Online]; available at INFN sez. Milano-Bicocca, Italy, June, 2018, http://www.sr-niel.org/.